Robotica (2013) volume 31, pp. 1275–1283. © Cambridge University Press 2013
doi:10.1017/S0263574713000507

Active control of flexible one-link manipulators using wavelet networks

V. I. Gervini†, E. M. Hemerly‡ and S. C. P. Gomes†*

†*Applied Mathematics and Control Laboratory, Federal University of Rio Grande (FURG), Av. Itália Km 8, 96201-900, Rio Grande, RS, Brazil*
‡*Technological Institute of Aeronautics (ITA), Electronics Division Praça Marechal Eduardo Gomes 50, 12228-900, São José dos Campos, SP, Brazil*

(Accepted May 1, 2013. First published online: June 7, 2013)

SUMMARY
The design of control laws for flexible manipulators is known to be a challenging problem, when using a conventional actuator, i.e., a motor with gear. This is due to the friction of the nonlinear actuator, which causes torque dead zone and stick-slip behavior, thereby hampering the good performance of the control system. The torque needed to attenuate the vibrations, although calculated by the control law, is consumed by the friction inside the actuator, rendering it ineffective to the flexible structure control. Nonlinear friction varies with different operational conditions of the actuator and a friction compensation mechanism based on these models cannot always keep a good performance. This study proposes a new control strategy using wavelet network to friction compensation. Experimental results obtained with a flexible manipulator attest to the good performance of the proposed control law.

KEYWORDS: Flexible robots; Wavelet networks; Friction; Control; Modeling.

1. Introduction

The main purpose of this paper is to present a new control strategy to solve a long-lasting and difficult problem: to eliminate vibration in flexible manipulators by using conventional nonlinear actuators. The friction in this type of actuator prevents the attainment of good performance by the control law.[1] As will be shown later, the necessary torque to eliminate the vibrations is sometimes inside the actuator torque dead zone, bounded by negative and positive static friction. In this region of low speeds, the phenomenon of stick-slip also exists. This combination of phenomena associated with the nonlinear friction at low speeds is definitely harmful to the performance of any control law proposed to eliminate structural vibrations.[2]

Several studies have been published about friction in robotic actuators. Most of them offer new types of friction models, as well as new ways to compensate friction from models.[3–6] The hardest problem associated with friction compensation based on friction models is that there are parametric variations in the actuator real friction. These parametric variations can sometimes cause great loss of performance in the friction compensation mechanism.

The main contribution of this work is the proposition of a control law that tries to compensate all dynamic nonlinearity, by means of identification through a WN. Traditional friction models reproduce the mean behavior of the phenomenon, but do not deal with the real-time variations of their parameters. The adaptive characteristic of the WN control is mainly used to compensate the nonlinear friction of the actuator, even in the presence of important parametric variations. As it will be verified later from experimental results, the proposed control strategy provides a good solution for the difficult problem regarding active control of flexible structures from conventional nonlinear actuators. The new result consists of proposing the use of wavelet networks (WNs) to identify the actuator's nonlinear friction and after this identification, the friction is rejected in order to enable the effective attenuation of the structural vibration by the control law with state feedback. Many authors have attempted to compensate friction from models, but the results are not satisfactory due to parametric variations (friction varies with time and operating conditions of the actuator). The compensation mechanism based on a WN is self-adaptive and can always keep a good performance in the rejection of nonlinear friction. To attenuate vibrations in flexible structures from actuators with nonlinear friction is still an open problem. The torque dead zone and stick-slip behavior prevent the control law to suppress vibrations. The control procedure proposed in this paper (control with state feedback and friction compensation using wavelet neural networks) solved this difficult problem. Other contributions of this paper that can be enhanced are the experimental validation of the control procedure and the theoretical proof of its stability.

In 1980s, some papers began to report studies that dealt with applications to robot manipulators with flexible links.[8] Since these studies were theoretical and showed only simulated results, the major problem in the active control of flexible structures has not become noticeable yet: the nonlinearities associated with the internal frictions of the actuators that prevent the good performance of the control laws. Schmitz[8] and Cannon and Rosenthal[9] studied the active control problem of a robot with only one flexible link and these studies considered experimental results. Mahmood *et al.*[10] presented experimental results for step response to

* Corresponding author. E-mail: sebastiaogomes@furg.br

https://doi.org/10.1017/S0263574713000507 Published online by Cambridge University Press

the tip position of a flexible manipulator using resonant control. However, in these experiments they used actuators without gear reduction (direct-drive). Gomes and Chrétien[4] highlighted the real problem, i.e., the control of one flexible structure by employing a conventional motor with gear actuator. In 2006, Gomes *et al.*[11] proposed the use of a friction compensation mechanism based on a neural network with offline training and showed good results. However, how to solve the problems related to changes in the friction parameters was not suggested. Some more recent works make the use of piezoelectric actuators for active vibration control. Qiu[12] proposed a control that uses piezoelectric acceleration sensor to suppress the unwanted vibration for flexible joint and flexible link robot.

One of the first studies of WN was proposed in 1992.[13] Since then, several studies have been published on the subject, specifically applied to control systems. Applications to robotics began to emerge in recent years. Sun *et al.*[14] proposed WN trained with back propagation for the identification of a two-link manipulator model. Naerum *et al.*[15] used WN for the identification of friction in the joints of a manipulator with rigid links. Cheng[16] developed an end-point control to a flexible manipulator, based on WNs and this proposition showed better simulation results when compared with the PD control. Dongbing and Huosheng[17] proposed a WN to the control of a mobile robot with nonlinearity, uncertainty and they showed good simulation results. Sung *et al.*[18] developed a robust control applied to flexible-joint robots, based on a self-recurrent WN and presented good simulation results. Houglin and Nair[19] proposed a WN to identify and compensate friction at low velocities and showed evidences by experimental results. Ming *et al.*[20] showed, from simulation results, a WN applied to high-precision position control of flexible joint with nonlinear friction.

This paper shows the results of an original application of WN to eliminate the structural vibrations of flexible robots, more precisely, in a robot manipulator with a single flexible link. This paper is structured as follows. The experimental setup is described in Section 2; actuator and structural model in Sections 3 and 4, respectively; Section 5 shows open loop results; the WN control is introduced in Section 6; Section 7 shows control stability analysis and the experimental results are presented and discussed in Section 8.

2. The Flexible Manipulator

The flexible robot manipulator described in this paper was constructed at the Applied Mathematics and Control Laboratory, located at the Federal University of Rio Grande, Brazil. A picture of this manipulator can be seen in Fig. 1. This manipulator comprises a very flexible beam, made of aluminum, free at one extremity (end effector), and articulated at the other (motor with gear drive joint). Three strain gauge sensors were placed on the flexible beam and provided angular deformation measures at selected points, as explained in Section 3. This number of strain gauges was used because the second flexible mode is well visible in the experiments and the interest is the control of the first two flexible modes. An encoder was used to provide the rotor angular position. The physical parameters of the flexible

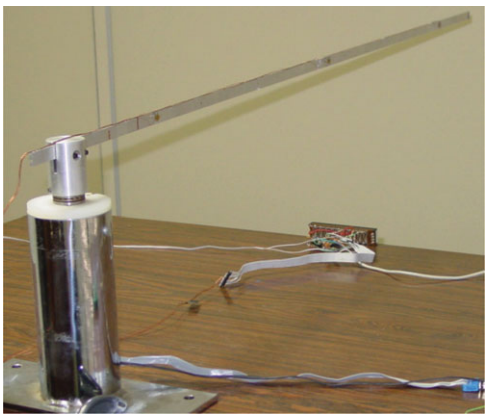


Fig. 1. (Colour online) Picture of the flexible manipulator.

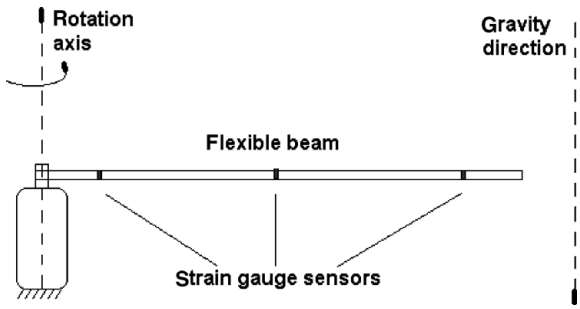


Fig. 2. Geometric representation of the flexible manipulator.

manipulator are the following (in this paper, all variables and parameters have physical units defined at the actuator load output axis side):

$$I_r = 0.01334\ \text{kgm}^2; \quad EI = 1.975\text{Nm}^2; \quad m_b = 0.1112\,\text{kg};$$
$$l = 1.1\ \text{m}; \quad h = 0.0126\,\text{m}; \quad e = 0.00305\ \text{m},$$

where I_r is the rotor inertia, EI is the Young's modulus multiplied by the cross section of straight beam, l, m_b, h, and e are the length, mass, height, and thickness of the flexible beam, respectively. Figure 2 shows the geometric representation of the flexible manipulator, indicating that the most important flexibility occurs on the horizontal plane. A harmonic-drive actuator was used; this type of actuator is very common in robotics, because it exhibits no considerable backlash. However, this actuator has an important torque dead zone due to the nonlinear friction. Table I lists the physical characteristics of the harmonic drive used in this study. There is no difficulty to attenuate the structural vibrations using a direct drive, because this type of actuator has an insignificant torque dead zone. Nevertheless, there is no practical interest in using direct drive due to its small

Table I. Harmonic-drive physical parameters.

Parameter	Numerical value
Rotor inertia (I_r)	0.01334 Kg m^2
Gear ratio (η)	100
Torque/current constant	1.74 Nm A^{-1}
Encoder resolution (load side)	50,000 ppr

https://doi.org/10.1017/S0263574713000507 Published online by Cambridge University Press

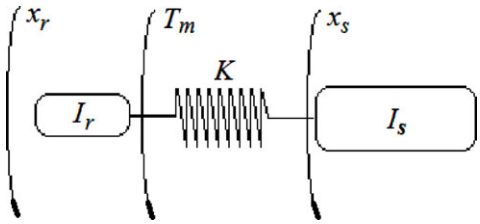


Fig. 3. Actuator with one flexible mode.

torque autonomy. The true challenge is to project control laws to attenuate the structural vibrations with actuators that use gearboxes. This is the underlying reason for using a harmonic drive in this study.

3. Actuator Dynamic Model

A geared motor drive joint robotic actuator can be visualized as a motion transmitter element containing an internal elasticity with constant K, as represented in Fig. 3. Equation (1) describes the dynamics of this system.[4] τ_m is the motor torque, I_r and I_s are the rotor and load inertia, respectively, τ_{at} is the nonlinear friction torque, x_r and x_s are the rotor and load angular positions, and η is the gear ratio.

$$I_r\,\ddot{x}_r + \frac{K}{\eta^2}(x_r - \eta x_s) = \tau_m - \tau_{at},$$
$$I_s\,\ddot{x}_s - K\left(\frac{x_r}{\eta} - x_s\right) = 0. \tag{1}$$

When a rigid approximation is considered, then $x_r/\eta = x_s$. System (1) reduces to

$$(\eta^2 I_r + I_s)\,\ddot{x}_s = \eta\,(\tau_m - \tau_{at}) \Rightarrow I_t\ddot{x}_s = T_m - T_{at}, \tag{2}$$

where I, T_m, and T_{at} are the total inertia, motor torque, and friction torque, respectively, with physical units at the gear output axis side. This rigid approximation can be assumed for friction torque identification purposes, since the drive joint internal flexibility generates a natural frequency of approximately 58 Hz, larger than the third dynamic vibration mode (39.8 Hz). The natural frequency of 58 Hz is due the speed reducer (gear), and it was obtained from experiments with the output shaft of the gear blocked. A torque sensor (based on strain gauges) was adapted at the gear output shaft. A motor torque of 1.74 Nm (maximum torque) was applied during 0.05 s. After this time, it was applied −1.74 Nm during the next 0.05 s, and a null torque after that. The signal analysis of the torque sensor showed the frequency of 58 Hz. However, it was found that the torque sensor was principally responsible for this frequency. The control law proposed in this paper did not use the torque sensor, and closed-loop experiments shown in this paper were made without this sensor. Therefore, the frequency of the actuator actually used in the experiments is certainly greater than 58 Hz and then, the rigid approximation used in the model (for the actuator) is well acceptable.

The friction model used in this study was proposed by Gomes and Rosa,[5] and it has two main objectives: to write the friction torque in the differential equation as an internal dynamic effect, instead of as an external torque; and to reproduce friction nonlinearity associated with torque dead zone and stick-slip behavior. The friction torque is written, as an internal dynamic effect, in the form:[11]

$$T_{at} = f_v^*\dot{x}_s, \tag{3}$$

where f_v^* is the variable viscous friction coefficient, obtained from an algorithm presented in ref. [11]. This algorithm indicates that f_v^* depends on the angular position, angular speed, and motor torque. From Eq. (3), Eq. (2) can be rewritten as

$$I_t\ddot{x}_s + f_v^*(x_s, \dot{x}_s, T_m)\,\dot{x}_s = T_m, \tag{4}$$

or in the following state form:

$$\begin{pmatrix}\dot{x}_s\\ \ddot{x}_s\end{pmatrix} = \begin{bmatrix}0 & 1\\ 0 & -\dfrac{f_v^*(x_s, \dot{x}_s, T_m)}{I_t}\end{bmatrix}\begin{pmatrix}x_s\\ \dot{x}_s\end{pmatrix} + \begin{pmatrix}0\\ \frac{1}{I_t}\end{pmatrix}T_m\,. \tag{5}$$

Equation (5) indicates that all nonlinearity associated with the friction is part of the dynamic matrix, unlike other models that consider friction as an external effort (motor effort).

The model presented in this study was obtained for a motor drive joint with harmonic drive and gear ratio $\eta = 100$, but the same modeling process can be applied to any motor drive joint of robots. Physical argumentations and more details about this issue are given in ref. [11].

4. Structural Dynamic Model

The lumped mass approach was used to obtain the dynamic structural model. In this approach, the continuum flexibility is replaced by a discrete approximation. A certain number of fictitious joints (considered placed at same positions of the fictitious joints shown in Fig. 3) are considered to connect the rigid parts of the beam.[21] Once the fictitious joints are placed, the Euler–Lagrange formalism is used to obtain the differential equations of the flexible manipulator. Including the actuator dynamics, it assumes the form:

$$[I]\,\ddot{\vec{x}} + [C_{at}]\dot{\vec{x}} + [K_{el}]\vec{x} + [B']T_{at}(\vec{x}, \dot{\vec{x}}, T_m) = [B']T_m, \tag{6}$$

where $[I]_{\alpha+1,\alpha+1}$ is the inertia matrix, $[K_{el}]_{\alpha+1,\alpha+1}$ is the elastic constants matrix, $[C_{at}]_{\alpha+1,\alpha+1}$ is the viscous friction coefficients matrix, $[B']_{1,\alpha+1} = [\,1\;0\cdots 0\,]^T$, α is the number of fictitious joints (it was considered $\alpha = 3$ in this study), $T_{at}(\vec{x}, \dot{\vec{x}}, T_m)$ is the actuator friction torque that concentrates all nonlinearity and $\vec{x} = [\,x_1\;x_2\;x_3\;x_4\,]^T$, where $x_1 = x_s$ (rotor angular position, encoder signal) and x_2, x_3, and x_4 are the fictitious joint angles (strain gauge sensor signals). The procedure to identify the elements of the matrix $[K_{el}]_{\alpha+1,\alpha+1}$ was as follows. Experiments were initially performed in an open loop with the rotor locked, and the Fast Fourier transform (FFT) was used to identify the natural frequencies of vibration modes corresponding

https://doi.org/10.1017/S0263574713000507 Published online by Cambridge University Press

to the cantilevers modes. Subsequently, the elements of the matrix $[K_{el}]_{\alpha+1,\alpha+1}$ were estimated, so that the zeros of the open-loop transfer function $\theta_1(s)/T_m(s)$ coincided with the frequencies identified experimentally (θ_1 is the rotor angular position). The parameters of the $[C_{at}]_{\alpha+1,\alpha+1}$ matrix were identified through the open-loop experimental results, by comparing them with the simulated ones to ensure that the simulated oscillations have the same decay as observed in the experimental results. An algorithm[21] gives all the matrices of Eq. (6) in a simple way. Equation (6) is the complete manipulator model, including the actuator and the structural dynamics, and it can be rewritten in the state space form as

$$\dot{\vec{X}} = A(\vec{X}, T_m)\vec{X} + BT_m\,. \tag{7}$$

The state vector in Eq. (7) has $2(\alpha+1)$ components, namely $\vec{X} = (x_1 \;\; x_2 \;\; x_3 \;\; x_4 \;\; \dot{x}_1 \;\; \dot{x}_2 \;\; \dot{x}_3 \;\; \dot{x}_4)^T$.

When considering a linear approximation to the dynamics of the actuator (nonlinear friction is null), the viscous friction coefficient in Eq. (5) becomes constant and the manipulator dynamics is written in the state form as

$$\dot{\vec{X}} = A\vec{X} + BT_m$$

with A and B constants.

The dynamic model approach adopted in this paper is very useful for deciding where to locate the strain gauge sensors along the beam: they are placed exactly at the fictitious joint positions. The dynamic modeling approach and the strategy of positioning the sensors allow full state observation, thereby avoiding the utilization of state estimation.

5. Open-Loop Results

The average static friction torque was identified as being equivalent to 10.8% of the maximum actuator motor torque and this limit defines the torque dead zone. It means that any torque below 10.8% of the maximum motor torque will not generate motion of the actuator load output axis. This value was identified by applying a motor torque increasing slowly from zero. From the historical time of the motor torque and encoder signal (encoder coupled to rotor), it is possible to verify the torque required to start the rotor angular motion. This is the static friction, which defines the torque dead zone. This experiment was repeated several times, and the average static friction torque was calculated, equal to 10.8% of the actuator maximum torque. In ref. [11], it was shown that the control torque necessary to attenuate the structural vibration has an amplitude level into the torque dead zone and this means impossibility of attenuating structural vibrations with active control, without any friction compensation strategy.

Figure 4 shows a confrontation between the simulation and the experiment for open-loop operation. A step motor torque equal to 50% of the maximum torque was applied during the first 0.05 s, −50% at the following 0.05 s, and a null torque up to 0.1 s. The simulation and the experimental results are given in Fig. 4, related to the tip angular position

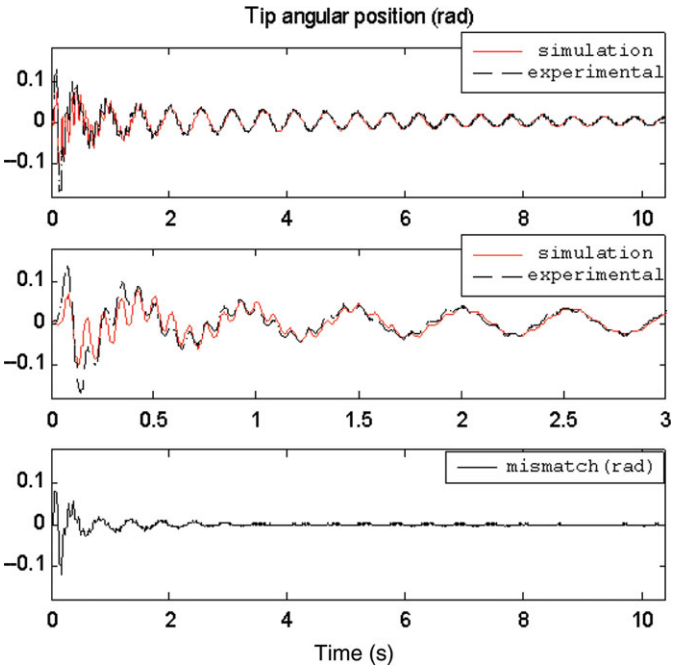


Fig. 4. (Colour online) Experimental and simulation results in open loop.

Table II. Open-loop poles and zeros.

Zeros	$-0.0057 \pm 12.1i$; $-0.658 \pm 76.19i$; $-4.169 \pm 247.89i$
Poles	0; -1.78; $-2.55 \pm 23.6i$; $-0.87 \pm 78.72i$; $-4.35 \pm 249.99i$

(x_4). In this figure, a zoom related to the first 3 s and the mismatch among the experimental and the simulation results are also shown. The simulation was performed using the nonlinear model (7). The dynamic model (structure and actuator) reproduces the experimental result well, since the two first structural flexible modes are quite noticeable. These modes have the cantilevers frequencies, equivalent to the zeros frequencies of the collocated open-loop transfer function.[22] When the actuator is in stick mode, the rotor is locked, i.e., the rotor velocity is zero, and this means that the dynamic system vibrates with the cantilevers modes. The application of the FFT to the load angular position signal can be seen in Fig. 5, and the frequencies that appear in the FFT are the cantilevers modes. The open-loop poles and zeros of the model are shown in Table II. The lowest frequency observed in the experimental result in Fig. 4 corresponds to 12.1rads^{-1}.

6. Biased Wavelet Network Control

6.1. Parameterization adopted

The WNs are able to approximate any continuous function. In WN's approaches, any finite-energy signal can be described as a linear combination of wavelets at different resolution levels.[13] The biased WN employed here is parameterized

https://doi.org/10.1017/S0263574713000507 Published online by Cambridge University Press

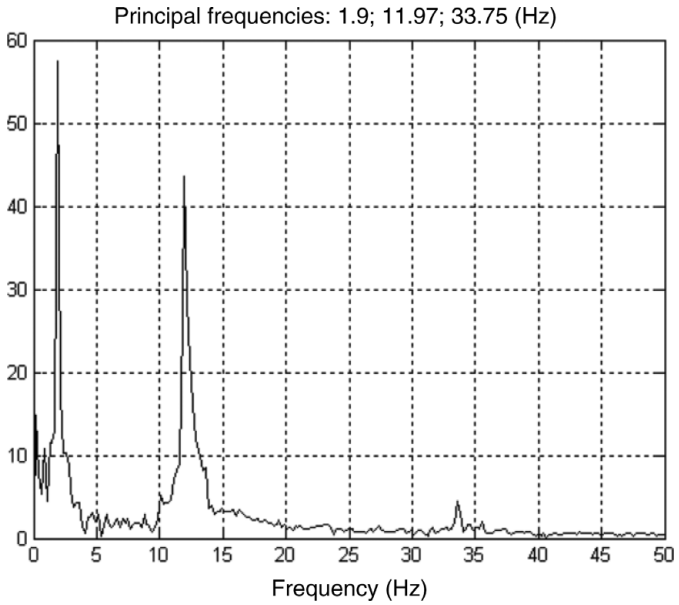


Fig. 5. FFT applied to the tip angular position signal of Fig. 4, after the first 0.5 s.

as

$$y_i = \sum_{j=1}^{Nh}\left[\omega_{ij}\psi\left(\sum_{k=1}^{n} v_{jk}\zeta_k + \theta_{vj} - d_j\right) + \theta_{\omega i}\right] + \sum_{j=1}^{Nh}\left[u_{ij}\varsigma\left(\sum_{k=1}^{n} v_{jk}\zeta_k + \theta_{vj} - d_j\right) + \theta_{ui}\right], \quad (8)$$

where y_i is the ith WN's output, n is the number of input variables, $\psi(.)$ is the wavelet function, $\varsigma(.)$ is the bias function (to be detailed later), N_h is the number of hidden wavelet nodes ("wavelons"), v_{jk} (which can be interpreted as a dilation parameter) is the interconnection weight from kth input to the jth wavelon, ω_{ij} and u_{ij} are the interconnection weight from the jth wavelon to the ith output node, and d_j is the translation parameter. θ_{vj} and θ_{wj} are offset values for the input-wavelon and wavelon-output connections, respectively. The network structure is depicted in Fig. 6. For the convenience of visualization, only one wavelon and one output are displayed. The parameters θ_{vj} and d_j as well as θ_{wj} and θ_{ui} are not grouped to simplify the matrix representation (see Section 6.2).

The term "biased" is due to the inclusion of a bias function $\varsigma(.)$ in the wavelet node. Unlike the wavelet $\psi(.)$, this function is required to have a nonzero mean in order to reproduce low-frequency features more easily. Its use was proposed in ref. [23] as a surrogate for a scaling function.[24] In fact, WN's representations usually employ differentiable wavelets with simple explicit expressions in order to simplify the derivation of gradient expressions.[13] However, in general such wavelets do not have an associated scaling function and, as a result, a large number of multiresolution levels may be required to reduce the approximation error.[24] Good results[23] were obtained for data compression using the biased wavelet representation, a fact that encourages its use in other domains.

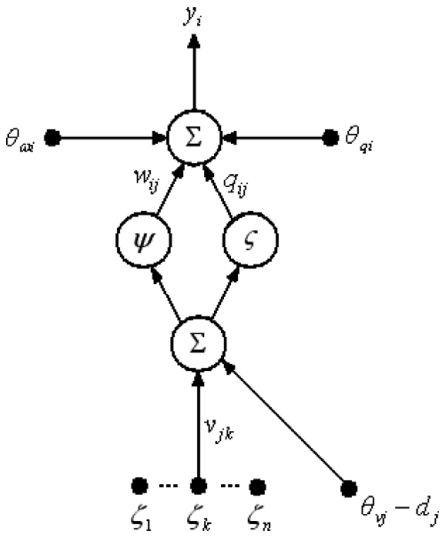


Fig. 6. Connection between the kth wavelon and the ith output of the biased wavelet network.

According to ref. [23], a prospective bias function should satisfy

(i) $\varsigma \in L^2(\Re)$;
(ii) $\breve{\varsigma}(0) \neq 0$;
(iii) $|\varsigma(\cdot)|$ is rapidly decreasing to zero when $|\cdot| \to \infty$;
(iv) $|\breve{\varsigma}(\cdot)|$ is rapidly decreasing to zero when $|\cdot| \to +\infty$,

where $\breve{\varsigma}(\cdot)$ is the Fourier transform of $\varsigma(\cdot)$. These requirements are needed to preserve the space-frequency localization properties of the WNs, while allowing an easier representation of low-frequency features. In this study, the bias function was chosen as $\varsigma(z) = e^{-\frac{z^2}{2}}$ because it has good representation in time and frequency, and the used wavelet function is $\psi(z) = \cos(2.5z)e^{-\frac{z^2}{2}}$, where$z \in \Re$. It should be emphasized that the use of bias does not interfere with the universal approximation property: it just adds more degrees of freedom.

6.2. *Matrix notation*

Equation (8) can be written in matrix notation as

$$y = W^T\psi(V^T\vec{\zeta} - D^T) + U^T\varsigma(V^T\vec{\zeta} - D^T), \quad (9)$$

where vector $\vec{\zeta}$ contains the input variables plus a unit input, i.e., $\vec{\zeta} = [\,1\ \zeta_1\ \zeta_2\ \ldots\ \zeta_n\,]^T$. The offset values and the connection weights are grouped in matrices W^T, V^T, D^T, and U^T, as

$$W^T = \begin{bmatrix} \theta_{w_1} & w_{11} & w_{12} & \cdots & w_{1N_h} \\ \theta_{w_2} & w_{21} & w_{22} & \cdots & w_{2N_h} \\ \vdots & \vdots & \vdots & \ddots & \vdots \\ \theta_{w_m} & w_{m1} & w_{m2} & \cdots & w_{mN_h} \end{bmatrix}_{m\times N_h+1},$$

$$V^T = \begin{bmatrix} \theta_{v_1} & v_{11} & v_{12} & \cdots & v_{1n} \\ \theta_{v_2} & v_{21} & v_{22} & \cdots & w_{2n} \\ \vdots & \vdots & \vdots & \ddots & \vdots \\ \theta_{v_{N_h}} & v_{N_h1} & v_{N_h2} & \cdots & w_{N_hn} \end{bmatrix}_{N_h\times n+1},$$

https://doi.org/10.1017/S0263574713000507 Published online by Cambridge University Press

$$D^T = \begin{bmatrix} d_1 \\ \vdots \\ d_{N_h} \end{bmatrix}_{N_h \times 1},$$

$$U^T = \begin{bmatrix} \theta_{u_1} & u_{11} & u_{12} & \cdots & u_{1N_h} \\ \theta_{u_2} & u_{21} & u_{22} & \cdots & u_{2N_h} \\ \vdots & \vdots & \vdots & \ddots & \vdots \\ \theta_{u_m} & u_{m1} & u_{m2} & \cdots & u_{mN_h} \end{bmatrix}_{m \times N_h + 1},$$

and the operators ψ and ς now yield vectors with the output values of the wavelet and bias functions for each wavelon, augmented with a unit output, such as in vector $\vec{\zeta}$.

6.3. Dynamic controller

Observing Eq. (6) and adopting $f(\vec{\zeta}) = T_{at}(\vec{x}, \dot{\vec{x}}, T_m)$ (unmodeled actuator nonlinear friction), it can be represented using WNs as

$$f(\vec{\zeta}) = W^T \psi(V^T \vec{\zeta} - D^T) + U^T \varsigma(V^T \vec{\zeta} - D^T) + \varepsilon, \quad (10)$$

where ε is the approximation error, defined as $\varepsilon = f(\vec{\zeta}) - \hat{f}(\vec{\zeta})$. The input vector $\vec{\zeta}$ is here composed by $\vec{\zeta} = [\,1 \;\; x_1 \;\; x_2 \;\; x_3 \;\; x_4 \;\; \dot{x}_1 \;\; \dot{x}_2 \;\; \dot{x}_3 \;\; \dot{x}_4 \;\; T_m\,]^T$.

The WN's application in this case is relevant, because it is usually very difficult to calculate the nonlinear actuator friction, or it may change with the time and operating conditions. The following control law is then proposed as

$$T_m = \hat{f}(\vec{\zeta}) + r - \nu \quad (11)$$

where $\hat{f}(\vec{\zeta})$ is an estimation of $f(\vec{\zeta})$, ν is the robustifing term defined in Section 7 (stability proof), and r is the linear system closed-loop control given as follow

$$r = K_r \cdot \vec{e} = [\,K_p \;\; K_d\,] \cdot \begin{bmatrix} \vec{x}_e \\ \dot{\vec{x}}_e \end{bmatrix} = K_p \vec{x}_e + K_d \dot{\vec{x}}_e \quad (12)$$

with the error $\vec{e}$ defined as

$$\vec{e} = \begin{bmatrix} \vec{x}_e \\ \dot{\vec{x}}_e \end{bmatrix} = \begin{bmatrix} \vec{x}_{ref} - \vec{x} \\ \dot{\vec{x}}_{ref} - \dot{\vec{x}} \end{bmatrix}, \quad (13)$$

where $\vec{x}_{ref}$ end $\dot{\vec{x}}_{ref}$ are reference position and velocity.

Equation (12) can be seen as a state feedback control (r) that employs a WN compensation of all system nonlinearity ($\hat{f}(\vec{\zeta})$). So, if $\hat{f}(\vec{\zeta})$ is obtained via WNs, then Eq. (11) can be rewritten as

$$T_m = \hat{W}^T \psi(\hat{V}^T \vec{\zeta} - \hat{D}^T) + \hat{U}^T \varsigma(\hat{V}^T \vec{\zeta} - \hat{D}^T) + r - \nu. \quad (14)$$

The coefficients of the WNs are updated according to Eqs. (15)–(18):

$$\dot{\hat{W}} = M \hat{\psi} r - M \hat{\psi}'(\hat{V}^T \vec{\zeta} - \hat{D}^T) r - k\,|r|\, M \hat{W}, \quad (15)$$

$$\dot{\hat{V}} = N \vec{\zeta} \hat{W}^T \hat{\psi}' r + N \vec{\zeta} \hat{U}^T \hat{\varsigma}'^T r - k\,|r|\, N \hat{V}, \quad (16)$$

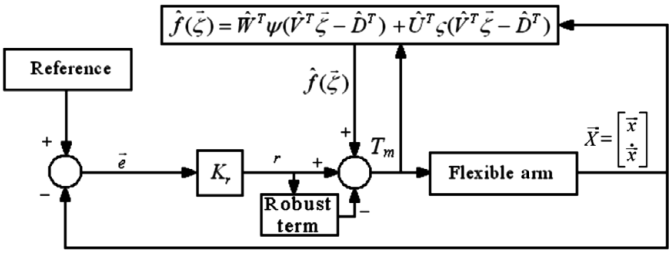


Fig. 7. Block diagram of the WN controller.

$$\dot{\hat{D}} = -O \hat{W}^T \hat{\psi}' r - O \hat{U}^T \hat{\varsigma}'^T r - k\,|r|\, O \hat{D}, \quad (17)$$

$$\dot{\hat{U}} = P \hat{\varsigma}\, r - P \varsigma'(\hat{V}^T \vec{\zeta} - \hat{D}^T) r - k\,|r|\, P \hat{U}, \quad (18)$$

where M, N, O, and P are positive-definite matrices and k a positive constant, with $\hat{\psi} = \psi(\hat{V}^T \vec{\zeta} - \hat{D}^T)$, $\hat{\psi}' = \frac{\partial \hat{\psi}}{\partial t}$, $\hat{\varsigma} = \varsigma(\hat{V}^T \vec{\zeta} - \hat{D}^T)$, and $\hat{\varsigma}' = \frac{\partial \hat{\varsigma}}{\partial t}$.

The weights and biases are initialized randomly with null mean and variance 1 and biases are updated in each time step. The block diagram of the WN controller is presented in Fig. 7. The stability proof of this control law is shown in the next section.

7. Lyapunov-Like Analysis

The following Lyapunov function candidate is proposed:

$$L = \frac{1}{2} r^2 + \frac{1}{2} tr\{\tilde{W}^T M^{-1} \tilde{W}\} + \frac{1}{2} tr\{\tilde{V}^T N^{-1} \tilde{V}\} + \frac{1}{2} tr\{\tilde{D}^T O^{-1} \tilde{D}\} + \frac{1}{2} tr\{\tilde{U}^T P^{-1} \tilde{U}\}, \quad (19)$$

where $\tilde{W}$, $\tilde{V}$, $\tilde{D}$, and $\tilde{U}$ are the estimation errors of the weights of ideal matrices W, V, D, and U, respectively:

$$\tilde{W} = W - \hat{W} \rightarrow \dot{\tilde{W}} = -\dot{\hat{W}},$$
$$\tilde{V} = V - \hat{V} \rightarrow \dot{\tilde{V}} = -\dot{\hat{V}},$$
$$\tilde{D} = D - \hat{D} \rightarrow \dot{\tilde{D}} = -\dot{\hat{D}},$$
$$\tilde{U} = U - \hat{U} \rightarrow \dot{\tilde{U}} = -\dot{\hat{U}}.$$

Differentiating Eq. (19)

$$\dot{L} = r\dot{r} + tr\{\tilde{W}^T M^{-1} \dot{\tilde{W}}\} + tr\{\tilde{V}^T N^{-1} \dot{\tilde{V}}\} + tr\{\tilde{D}^T O^{-1} \dot{\tilde{D}}\} + tr\{\tilde{U}^T P^{-1} \dot{\tilde{U}}\}. \quad (20)$$

The term $\dot{r}$ is obtained by differentiating Eq. (12) and using dynamic model (6) (there is a similar procedure proposed in ref. [25]):

$$\dot{r} = -k_v r + \tilde{W}^T(\hat{\sigma} - \hat{\sigma}'(\hat{V}^T \zeta - \hat{D}^T)) + \hat{W}^T \hat{\sigma}'(\tilde{V}^T \zeta - \tilde{D}^T) + \tilde{U}^T(\hat{\varsigma} - \hat{\varsigma}'(\hat{V}^T \zeta - \hat{D}^T)) + \hat{U}^T \hat{\varsigma}'(\tilde{V}^T \zeta - \tilde{D}^T) + w + v, \quad (21)$$

https://doi.org/10.1017/S0263574713000507 Published online by Cambridge University Press

where k_v is a gain parameter, v is the robustifing term, given by

$$v = -k_z(\|\hat{Z}\|_F + Z_L)\, r \tag{22}$$

with k_z a positive constant, $\|\cdot\|_F$ the Frobenius norm, and Z defined by

$$Z \equiv \begin{bmatrix} W & 0 & 0 & 0 \\ 0 & U & 0 & 0 \\ 0 & 0 & V & 0 \\ 0 & 0 & 0 & D \end{bmatrix} \tag{23}$$

$w(t)$ is the disturbing term, given by

$$\begin{aligned} w = {} & \tilde{W}^T\hat{\sigma}'(\hat{V}^T\zeta - \hat{D}^T) + \hat{W}^T O(\tilde{V}^T\zeta - \tilde{D}^T)^2 \\ & + \tilde{U}^T\hat{\varsigma}'(\hat{V}^T\zeta - \hat{D}^T) + \hat{U}^T O(\tilde{V}^T\zeta - \tilde{D}^T)^2 + \varepsilon \end{aligned} \tag{24}$$

with $\varepsilon(\zeta)$ representing the reconstruction error of $f(\zeta)$ by the WN, and w is limited by

$$|w| \le c_0 + c_1\|\tilde{Z}\|_F + c_2|r|\|\tilde{Z}\|_F, \tag{25}$$

where c_i are positive constants.

From Eqs. (20) and (24)

$$\begin{aligned} \dot{L} = {} & -k_v r^2 + r\tilde{W}^T(\hat{\sigma} - \hat{\sigma}'(\hat{V}^T\zeta - \hat{D}^T)) \\ & + r\hat{W}^T\hat{\sigma}'(\tilde{V}^T\zeta - \tilde{D}^T) + r\tilde{U}^T(\hat{\varsigma} - \hat{\varsigma}'(\hat{V}^T\zeta - \hat{D}^T)) \\ & + r\hat{U}^T\hat{\varsigma}'(\tilde{V}^T\zeta - \tilde{D}^T) + tr\{\tilde{W}^T M^{-1}\dot{\tilde{W}}\} \\ & + tr\{\tilde{V}^T N^{-1}\dot{\tilde{V}}\} + tr\{\tilde{D}^T O^{-1}\dot{\tilde{D}}\} + tr\{\tilde{U}^T P^{-1}\dot{\tilde{U}}\} \\ & + rw + rv. \end{aligned} \tag{26}$$

Using Eqs. (15)–(18) in (26)

$$\dot{L} = -k_v r^2 + k\,|r|\,tr\{\tilde{Z}^T(Z - \tilde{Z})\} + rw + rv. \tag{27}$$

Noting that $rw \le |r||w|$, and assuming $k_Z > c_2$ and $Z_L > \|Z\|_F$

$$\dot{L} \le -|r|(K_v|r| - k\|\tilde{Z}\|_F Z_L + k\|\tilde{Z}\|_F^2 - c_0 - c_1\|\tilde{Z}\|_F), \tag{28}$$

$$\dot{L} \le -|r| \cdot g(r, \tilde{Z}). \tag{29}$$

To $\dot{L} < 0$, it is necessary that $g(r, \tilde{Z}) > 0$. Setting up

$$c_3 \equiv Z_L + \frac{c_1}{k}, \tag{30}$$

one obtains the equation

$$g(r, \tilde{Z}) = K_v|r| + k(\|\tilde{Z}\|_F - \frac{1}{2}c_3)^2 - \frac{k}{4}c_3^2 - c_0. \tag{31}$$

To ensure $g(r, \tilde{Z}) > 0$, it is necessary that

$$|r| > \frac{kc_3^2 + 4c_0}{4K_v}, \tag{32}$$

$$\|\tilde{Z}\|_F > \sqrt{\frac{kc_3^2 + 4c_0}{4k}} + \frac{c_3}{2}. \tag{33}$$

Equations (32) and (33) define a compact region, outside $\dot{L}$ is negative. This means that the variables contained in L (r e$\tilde{Z}$) are limited. This result corresponds to a type of stability called UUB (*uniformly ultimately bounded*) derived from the standard Lyapunov theorem.[26]. Equations (32) and (33) indicate UUB of $|r|$ and $\|\tilde{Z}\|_F$. In summary, r represents the control signal, which depends on the state feedback (see Eqs. (11) and (12)). $\tilde{Z}$ is a matrix composed by four matrices of network parameters errors, i.e., differences between ideal parameters (unknown) and current WN parameters. Equations (32) and (33) ensure that when the standards $|r|$ and $\|\tilde{Z}\|_F$ exceed certain constant values, the time derivative of the Lyapunov function becomes less than zero and ensures stability, i.e., the control signal and the errors in the WN parameters are thus limited.

8. Pseudo-algorithm of the Control Law

In this section, a pseudo-algorithm is presented in order to facilitate the implementation of the proposed control law, which uses a friction compensation based on online identification of nonlinear friction from a wavelet network (WN).

Initially, the gains vector of the state feedback control (K_r) is projected, using pole placement for linear dynamics of the flexible manipulator (linear approximation is considered for the dynamics of the actuator). Subsequently, the WN weights matrix $\hat{W}$,$\hat{V}$,$\hat{D}$, and $\hat{U}$ are initialized with small random values between 0 and 0.1, for instance. After these initializations, each discretization step control must contain the following:

- input vector of WN ($\vec{\zeta} = [1\ x_1\ x_2\ x_3\ x_4\ \dot{x}_1\ \dot{x}_2\ \dot{x}_3\ \dot{x}_4\ T_m]^T$), which is updated;
- calculated output of the WN ($\hat{f}(\vec{\zeta}) = \hat{W}^T\psi(\hat{V}^T\vec{\zeta} - \hat{D}^T) + \hat{U}^T\varsigma(\hat{V}^T\vec{\zeta} - \hat{D}^T)$), (functions ψ and ς were defined in Section 6);
- calculated linear control given in Eq. (12) ($r = K_r \cdot \vec{e}$), with $\vec{e}$ defined in Eq. (13);
- calculated the robustifing term from Eq. (22) ($v = -k_z(\|\hat{Z}\|_F + Z_L)r$), ($Z_L$must obey the relation $Z_L > \|Z\|_F$, k_z is a positive constant gain and Z is defined in Eq. (23));
- calculated torque control from Eq. (11) ($T_m = \hat{f}(\vec{\zeta}) + r - v$);
- after the application of the control torque, the adaptation of the WN weights should be made using Eqs. (15)–(18) ($\dot{\hat{W}} = M\hat{\psi}r - M\hat{\psi}'(\hat{V}^T\vec{\zeta} - \hat{D}^T)r - k|r|M\hat{W}$), ($\dot{\hat{V}} = N\vec{\zeta}\hat{W}^T\hat{\psi}'r + N\vec{\zeta}\hat{U}^T\hat{\varsigma}'^T r - k|r|N\hat{V}$), ($\dot{\hat{D}} = -O\hat{W}^T\hat{\psi}'r - O\hat{U}^T\hat{\varsigma}'^T r - k|r|O\hat{D}$), ($\dot{\hat{U}} = P\hat{\varsigma}r - P\varsigma'(\hat{V}^T\vec{\zeta} - \hat{D}^T)r - k|r|P\hat{U}$).

M, N, O, and P should be positive-definite matrices and k is a positive constant, defined in the project. It is important to know the flexible manipulator dynamic model and then, from simulations, to determine these WN parameters that

https://doi.org/10.1017/S0263574713000507 Published online by Cambridge University Press

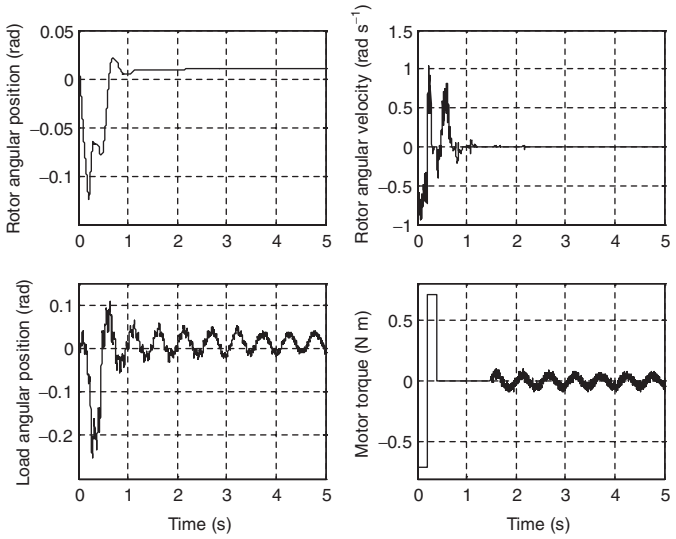


Fig. 8. Closed loop without wavelet network control.

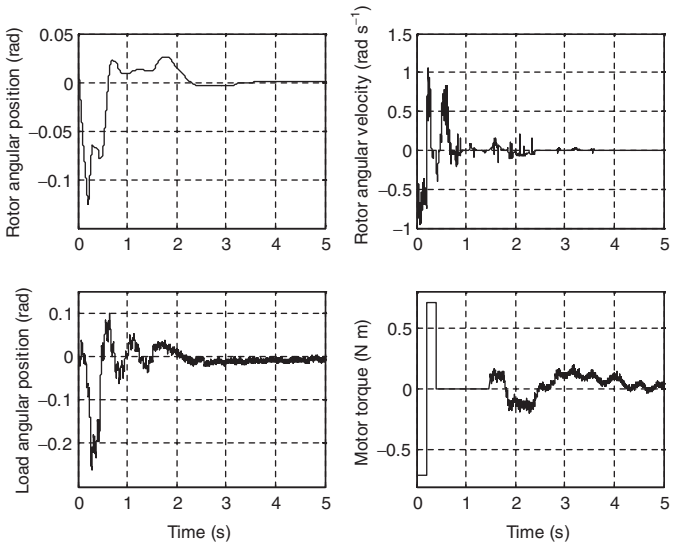


Fig. 9. Closed loop with wavelet network control (experiment 1).

allow a more rapid convergence in the online adaptation of the weights in Eqs. (15)–(18).

9. Experimental Close-Loop Results

The experimental results presented below were obtained with an initial excitation of the flexible modes in open loop. During the first 0.2 s, a torque of −0.7 N m was applied. Over the next 0.2 s, the torque was 0.7 N m, and it was zeroed until 1.5 s, the instant in which the torque is calculated by the closed-loop control. Figures 8–10 show the rotor angular position, the rotor angular velocity, the load angular position (tip angular position), and the motor torque. This type of experiment presents the greatest difficulty for the control law because the vibration needs to be damped (control of flexible modes) and the angular position of the base (rotor angular position) must return to zero after making a small shift in open loop (approximately 0:02 rad, control of the rigid mode).

Figure 8 shows the application of control with state feedback without using the WN compensation ($\hat{f}(\vec{\zeta})$). By observing the load angular position, oscillations that were not canceled by the control law can be seen. Although the motor torque calculated by the control law is not zero, it is fully within the torque dead zone of the actuator, bounded by the negative and positive static friction. Then, this control torque does not reach the flexible structure, which remains as a vibrating beam, fixed at one end and free at the other. In this situation, the rotor remains with zero angular velocity (stick mode).

Figure 9 shows a result with the same control of Fig. 8, but including the WN compensation. As can be seen from the load angular position, the control law was able to cancel the structural vibrations. As the state reference is null, the control leads both the load position and the rotor position to zero, unlike the result seen in Fig. 8, in which there is a steady state error in the rotor position. The WN network identified all the nonlinearity due to friction of the actuator and the compensation of this nonlinearity was performed with a good performance. This fact allowed a good performance of the control law: the rotor was placed

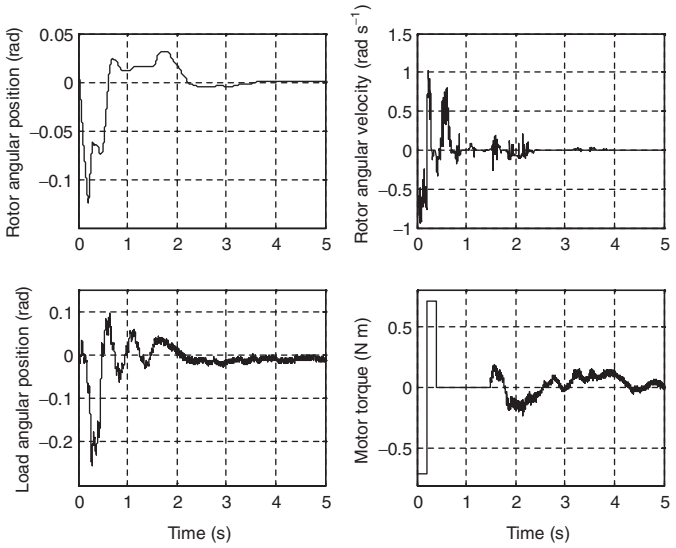


Fig. 10. Closed loop with wavelet network control (experiment 2).

to the zero position (reference position) and the structural vibrations were suppressed.

A question that arises immediately after this first closed-loop experiment is: would the control law be able to maintain the control performance even in the presence of friction parametric variations that occur in practice? To answer this question, several experimental results were obtained in closed loop, under different conditions. The most significant is to leave the actuator turned off for 24 h, after the actuator has worked for 10 min. This procedure ensures variations in the actuator friction. Figure 10 shows one of these results. It can be noticed that the performance was very similar to the one previously shown in Fig. 9.

One way to investigate numerically the control law performance is by carrying out a statistical analysis on the load angular position for several repeated experiments. Table III shows the correlation between four experiments. It can be seen that there was a high correlation among different experiments, thereby indicating that good performance is achieved by control law.

https://doi.org/10.1017/S0263574713000507 Published online by Cambridge University Press

Table III. Tip angular position correlation for four experimental closed-loop results.

	Exp. 1	Exp. 2	Exp. 3	Exp. 4
Exp. 1	1.0000	0.9915	0.9926	0.9896
Exp. 2	0.9915	1.0000	0.9923	0.9940
Exp. 3	0.9926	0.9923	1.0000	0.9927
Exp. 4	0.9896	0.9940	0.9927	1.0000

10. Conclusions

In the present paper, it was put in evidence the difficulty to eliminate vibrations in flexible structures from actuators with nonlinear friction. Variations in friction parameters are mainly dependent of the operation conditions and the fluid lubricant, such as physical characteristics and temperature. There is large evidence that it is hard to attenuate structural vibrations in an active control without solving the problems caused by nonlinear friction (torque dead zone and stick-slip behavior). Therefore, it is necessary to compensate friction to ensure good active control performance. As friction parameters may vary in time, to compensate them using a friction model can provoke loss of performance and hence, it is considered a partial solution. A good solution is provided in this paper, by means of adaptation: nonlinear friction can be identified and rejected using a WN. More precisely, the problem of active control of flexible manipulators from conventional actuators with nonlinear friction has been resolved. This is the main contribution, which represents a viable and efficient solution for the problem of active control of flexible structures, whose actuators have nonlinearities associated with friction. The proposed control law was always able to maintain good performance, even in the presence of significant variations in friction, that is, experiments performed with heated actuator showed performance equal with experiments performed with the actuator inactive during 24 h.

References

1. B. S. R. Armstrong, Dynamics for Robot Control: Friction Modeling and Ensuring Excitation During Parameter Identification *Ph.D. Dissertation* (California, USA: Stanford University, 1988).
2. V. I. Gervini, S. C. P. Gomes and V. S. Rosa, "A new robotic drive joint friction compensation mechanism using neural networks," *J. Braz. Soc. Mech. Sci. Eng. (ABCM)* **25**(2), 129–139 (2003).
3. C. Canudas de Wit, H. Olsson and K. Aströn, "A new model for control of systems with friction," *IEEE Trans. Autom. Control* **40**(3), 419–425 (1995).
4. S. C. P. Gomes and J. P. Chrétien, "Dynamic Modeling and Friction Compensated Control of a Robot Manipulator Joint," *Proceedings of IEEE Robotics and Automation Conference*, Nice, France (May 1992).
5. S. C. P. Gomes and V. S. Rosa, "A New Approach to Compensate Friction in Robotic Actuators," *Proceedings of IEEE International Conference on Robotics and Automation*, Taipei, Taiwan (Sep. 2003), vol. 1, pp. 622–627.
6. B. Bona and M. Indri, "Friction Compensation in Robotics: An Overview," *Proceedings of the 44th IEEE Conference on Decision and Control, and the European Control Conference 2005*, Seville, Spain (Dec. 12–15, 2005).
7. A. C. Bittencourt and S. Gunnarsson, "Static friction in a robot joint—modeling and identification of load and temperature effects," *J. Dyn. Syst. Meas. Control* **134**(5), **051013** (2012).
8. E. Schmitz, Experiments on the End-Point Control of a Very Flexible One-Link Manipulator *Ph.D. Dissertation* (California, USA: Stanford University, 1985).
9. R. H. Cannon and D. E. Rosenthal, "Experiments in control of flexible structures with noncolocated sensors and actuators," *J. Guid. Control* **7**(5), 546–553 (1984).
10. I. A. Mahmood, S. O. Reza Moheimani and B. Bhikkaji, "Positioning of a flexible manipulator using resonant control," *IEEE/ASME Trans. Mechatronics* **13**(2), 180–186 (2008).
11. S. C. P. Gomes, V. S. Rosa and B. C. Albertini, "Active control to flexible manipulators," *IEEE/ASME Trans. Mechatronics* **11**(1), 75–83 (2006).
12. Z. Qiu, "Acceleration Sensor Based Vibration Control for Flexible Robot by Using PPF Algorithm," *Proceedings of the IEEE International Conference on Control and Automation*, Guangzhou, China (May.–Jun. 2007) pp. 1335–1339.
13. Q. Zhang and A. Benveniste, "Wavelet network," *IEEE Trans. Neural Netw.* **3**, 889–898 (1992).
14. W. Sun, Y. Wang and J. Mao, "Using Wavelet Network for Identifying the Model of Robot Manipulator," *Proceedings of the 4th World Congress on Intelligent Control and Automation*, Shanghai, China, vol. 2, (Jun. 2002) pp. 1634–1638.
15. E. Naerum, J. Cornellà and O. J. Elle, "Wavelet Networks for Estimation of Coupled Friction in Robotic Manipulator," *Proceedings of the IEEE International Conference on Robotic and Automation*, Pasadena, CA, USA (May 2008).
16. D. X. P. Cheng, "End-Point Control of a Flexible Structure Mounted Manipulator Based on Wavelet Basis Function Networks," *Proceedings of the IEEE IROS Work Shop on Robot Vision for Space Application*, Alberta, Canada (Aug. 2005) pp. 29–34.
17. D. Gu and H. Hu, "Wavelet Neural Network Based Predictive Control for Mobile Robots," *Proceedings of the IEEE International Conference on System, Man and Cybernetics*, Nashville, TN (Oct. 2000), vol. 5, pp. 3544–3549.
18. J. Y. Sung, B. P. Jin and H. C. Yoon, "Adaptive Dynamic Surface Control of Flexible-Joint Robots Using Self-Recurrent Wavelet Neural Networks," *Proceedings of the IEEE International Conference on System, Man and Cybernetics*, Taipei, Taiwan (Dec. 2006) pp. 1342–1355.
19. D. Houglin and S. S. Nair, "Identification of Friction at Low Velocities Using Wavelet Basis Function Network," *American Control Conference*, Philadelphia, PA (Jun. 1998), vol. 3, pp. 1918–1922.
20. C. Ming, J. Qing-xuan and S. Han-xu, "Robust tracking control of flexible joint with nonlinear friction and uncertainties using wavelet neural networks," *Intell. Comput. Technol. Autom.* **1**, 878–883 (2009).
21. C. C. Machado, A. E. Pereira, S. C. P. Gomes and A. E. De Bortoli, "A new algorithm to flexible manipulator dynamic modeling," *Control Autom Mag. Braz. Soc. Autom. (SBA)* **13**(2), 134–140 (2002).
22. D. K. Miu, "Physical interpretation of transfer function zeros for simple control systems with mechanical flexibilities," *J. Dyn. Syst. Meas. Control* **113**(3), 419–424 (1991).
23. R. K. H. Galvão, T. Yoneyama and T. N. Rabello, "Signal representation by adaptive biased wavelet expansions," *Digit. Signal Process.* **9**(4), 255–240 (1999).
24. I. Daubechies, *Ten Lectures on Wavelets* (Philadelphia, PA: SIAM, 1992).
25. A. Yesildirek, M. W. Vandegrift and F. L. Lewis, "A Neural Network Controller for Flexible-Link Robots," *Proceedings of the IEEE International Symposium on Intelligent Control*, Columbus, OH (Aug. 1994) pp. 63–68.
26. F. L. Lewis, C. T. Abdallah and D. M. Dawson, *Control of Robot Manipulators* (New York: Macmillan, 1993).
27. K. S. Narendra and A. M. Annaswamy, "A new adaptive law for robust adaptation without persistent excitation," *IEEE Trans. Autom. Control* **32**(2), 134–145 (1987).

https://doi.org/10.1017/S0263574713000507 Published online by Cambridge University Press